CHAPTER IV

NUMERICAL RESULTS

In this chapter, we demonstrate the accuracy and convergence behavior of approximate solutions and computational efficiency of the proposed numerical procedure in the flexural buckling analysis of various structures, and a set of selected results is reported and discussed. To verify both the formulation and numerical implementation of the current technique, several examples whose analytical solution exists are first considered in numerical experiments. Once the method is tested, it is then applied to analyze more complex structures to demonstrate their capability. The number of adaptive steps (N) and the number of iterations required in the computation of the minimum eigenvalue in each iterative step ($\tilde{n}$) are also reported to indicate the computational cost.

4.1 Single column with various end conditions

Consider a perfectly straight column of length L, Young modulus E, moment of inertia I, and subjected to axial load P and various end conditions as shown in Figure 4.1. In the analysis, only one member is employed in the discretization and we choose the reference stress σ_0 = 35143581 kg/m^2, the reference strain ε_0 = 0.00172405, I = 0.00013333 m^4, A = 0.04 m^2 and L = 1 m. The percent error of the approximation ($|P_{current}-P_{exact}|/ P_{exact}*100$), the number of adaptive steps (N) and iterations required for eigen computation ($\tilde{n}$) are reported in Table 4.1-Table 4.6. Note that the exact elastic and inelastic buckling loads (P_{exact}) are given by $\pi^2EI / (KL)^2$ and $\pi^2E_TI / (KL)^2$, respectively, where the effective length factor (K) for each end condition can be readily found (e.g. Timoshenko and Gere, 1961; Chajes, 1974) and the exact tangent modulus can be computed from equation (3.10). It is evident that the numerical solutions are in excellent agreement with the analytical solutions. Only few adaptive steps are required to achieve the converged buckling load. In addition, by using the converged eigenvector from the previous adaptive step as an initial guess in the current step, computation of the minimum eigenvalue also requires only a few iterations.

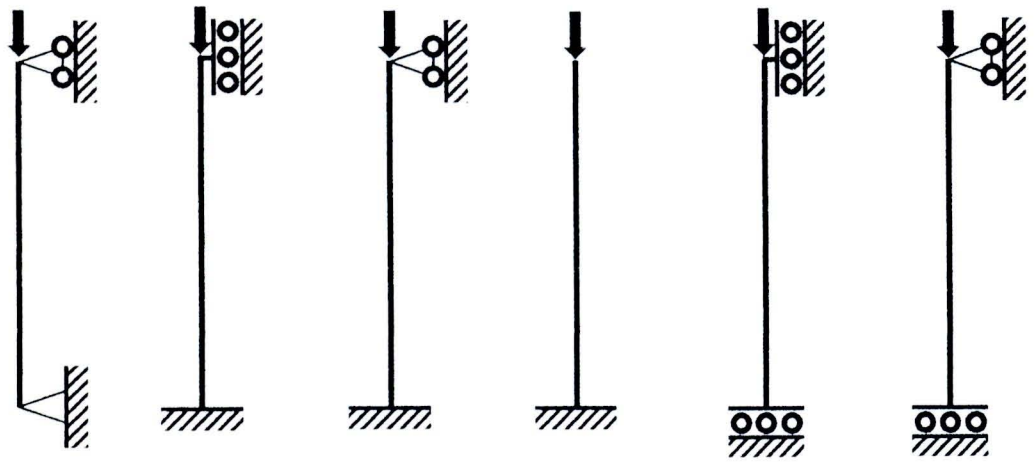

Figure 4.1 Schematic of single column subjected to (a) pined-pined conditions, (b) fixed-fixed conditions, (c) fixed-pinned conditions, (d) fixed-free conditions, (e) guided-fixed conditions, and (f) guided-pinned conditions

Table 4.1 Percent error of the approximation ($|P_{current}-P_{exact}|/ P_{exact}*100$) and number of adaptive steps and required iterations for minimum eigenvalue calculations for column with pinned-pinned condition

	Elastic buckling	Inelastic Buckling		
		n = 2, B = 0.5	n = 5, B = 0.8	n = 10, B = 0.9
N	Error (%), ($\tilde{n}$)	Error (%), ($\tilde{n}$)	Error (%), ($\tilde{n}$)	Error (%), ($\tilde{n}$)
1	17.694560, (7)	414.339097, (8)	1145.255513, (8)	1572.327132, (9)
2	0.802960, (2)	7.098078, (2)	11.515300, (2)	12.945235, (2)
3	0.001614, (2)	0.399663, (2)	0.636157, (2)	0.715591, (2)
4	0.000000, (2)	0.000816, (2)	0.001291, (2)	0.001452, (2)
5	0.000000, (2)	0.000000, (2)	0.000000, (2)	0.000000, (2)
6	-	0.000000, (2)	0.000000, (2)	0.000000, (2)

Table 4.2 Percent error of the approximation ($|P_{current}-P_{exact}|/ P_{exact}*100$) and number of adaptive steps and required iterations for minimum eigenvalue calculations for column with fixed-fixed condition

	Elastic buckling	Inelastic Buckling		
		n = 2, B = 0.5	n = 5, B = 0.8	n = 10, B = 0.9
N	Error (%), $(\tilde{n})$	Error (%), $(\tilde{n})$	Error (%), $(\tilde{n})$	Error (%), $(\tilde{n})$
1	1.088759, (6)	784.683240, (9)	3147.835950, (9)	4910.289796, (9)
2	0.000194, (2)	0.624544, (2)	0.997551, (2)	1.121576, (2)
3	0.000000, (2)	0.000130, (2)	0.000208, (2)	0.000234, (2)
4	0.000000, (2)	0.000000, (2)	0.000000, (2)	0.000000, (2)
5	-	0.000000, (2)	0.000000, (2)	0.000000, (2)

Table 4.3 Percent error of the approximation ($|P_{current}-P_{exact}|/ P_{exact}*100$) and number of adaptive steps and required iterations for minimum eigenvalue calculations for column with fixed-pinned condition

	Elastic buckling	Inelastic Buckling		
		n = 2, B = 0.5	n = 5, B = 0.8	n = 10, B = 0.9
N	Error (%), $(\tilde{n})$	Error (%), $(\tilde{n})$	Error (%), $(\tilde{n})$	Error (%), $(\tilde{n})$
1	44.735537, (2)	804.615214, (2)	2614.932711, (2)	3816.580498, (2)
2	18.421494, (2)	1.546228, (2)	11.901119, (2)	15.098986, (2)
3	2.776489, (2)	5.559987, (2)	10.226254, (2)	11.731389, (2)
4	0.058582, (2)	1.308366, (2)	2.109775, (2)	2.377495, (2)
5	0.000026, (2)	0.029551, (2)	0.046815, (2)	0.052669, (2)
6	0.000000, (2)	0.000013, (2)	0.000021, (2)	0.000023, (2)
7	-	0.000000, (2)	0.000000, (2)	0.000000, (2)

Table 4.4 Percent error of the approximation ($|P_{current}-P_{exact}|/ P_{exact}*100$) and number of adaptive steps and required iterations for minimum eigenvalue calculations for column with fixed-free condition

	Elastic buckling	Inelastic Buckling		
		n = 2, B = 0.5	n = 5, B = 0.8	n = 10, B = 0.9
N	Error (%), ($\tilde{n}$)	Error (%), ($\tilde{n}$)	Error (%), ($\tilde{n}$)	Error (%), ($\tilde{n}$)
1	0.277732, (5)	119.032773, (6)	249.992397, (6)	309.180919, (6)
2	0.000006, (2)	0.140960, (3)	0.221625, (3)	0.249295, (3)
3	0.000000, (2)	0.000003, (2)	0.000005, (2)	0.000006, (2)
4	-	0.000000, (2)	0.000000, (2)	0.000000, (2)

Table 4.5 Percent error of the approximation ($|P_{current}-P_{exact}|/ P_{exact}*100$) and number of adaptive steps and required iterations for minimum eigenvalue calculations for column with guided-fixed condition

	Elastic buckling	Inelastic Buckling		
		n = 2, B = 0.5	n = 5, B = 0.8	n = 10, B = 0.9
N	Error (%), ($\tilde{n}$)	Error (%), ($\tilde{n}$)	Error (%), ($\tilde{n}$)	Error (%), ($\tilde{n}$)
1	1.088754, (2)	341.587385, (2)	969.559490, (2)	1336.374571, (2)
2	0.000194, (2)	0.539779, (2)	0.862363, (2)	0.969658, (2)
3	0.000000, (2)	0.000097, (2)	0.000155, (2)	0.000174, (2)
4	0.000000, (2)	0.000000, (2)	0.000000, (2)	0.000000, (2)
5	-	-	0.000000, (2)	0.000000, (2)

Table 4.6 Percent error of the approximation ($|P_{current}-P_{exact}|/ P_{exact}*100$) and number of adaptive steps and required iterations for minimum eigenvalue calculations for column with guided-pinned condition

	Elastic buckling	Inelastic Buckling		
		n = 2, B = 0.5	n = 5, B = 0.8	n = 10, B = 0.9
N	Error (%), ($\tilde{n}$)	Error (%), ($\tilde{n}$)	Error (%), ($\tilde{n}$)	Error (%), ($\tilde{n}$)
1	0.277732, (5)	119.032773, (6)	249.992397, (6)	309.180919, (6)
2	0.000006, (2)	0.140960, (3)	0.221625, (3)	0.249295, (3)
3	0.000000, (2)	0.000003, (2)	0.000005, (2)	0.000006, (2)
4	-	0.000000, (2)	0.000000, (2)	0.000000, (2)

4.2 Rigid frame and equivalent model with rotational spring

Next, consider a rigid frame consisting of a column and two beams as shown schematically in Figure 4.2(a). Length of the column, the left beam and the right beam are given by L, ρL and λL, respectively, where ρ and λ are length ratios; the flexural rigidity of the column, the left beam and the right beam are given by EI, γEI and μEI, respectively, where γ and μ are constants indicating the flexural rigidity ratio; and the vertical load P is applied to the top of column. To demonstrate the capability of the current technique to treat a concentrated rotational spring, we also consider two other equivalent models in the analysis for the buckling load of the column: one obtained by replacing the right beam by an elastic rotational spring with stiffness $3\mu EI/\lambda L$ at the top of the column as shown in Figure 4.2(b) and the other obtained by replacing both beams by an elastic rotational spring with stiffness $3\mu EI/\lambda L + 3\gamma EI/\rho L$ at the top of the column as shown in Figure 4.2(c). In the analysis, the three structural models are discretized using only 3, 2 and 1 elements, respectively. Computed elastic buckling loads, normalized such that $\hat{P}_{current}=P_{current}/(\pi^2EI/L^2)$, are reported in Table 4.7 along with the normalized exact solution $\hat{P}_{exact}=P_{exact}/(\pi^2EI/L^2)$ obtained from directly solving the differential equation and exact eigenvalue problem for several values of $\{\gamma, \rho, \mu, \lambda\}$.

In the inelastic buckling analysis, σ_0 = 24607437 kg/m^2, ε_0 = 0.00346535, I = 0.00636173 m^4, A = 0.28274 m^2 and L = 1 m are chosen. The normalized inelastic buckling loads are reported in Table 4.8 and Table 4.9 compared with the normalized exact solution for n = 4, B = 0.75 and n = 8, B = 0.875, respectively. The number of adaptive steps and the total number of iterations in the eigenvalue computation are also reported. As is clearly indicated for both elastic buckling and inelastic buckling, approximate solutions are comparable to the exact solution for all three models. In addition, the number of adaptive steps required to achieve the converged solutions for both elastic and inelastic cases is relatively few; in particular, the number of adaptive steps for the inelastic case is larger than that for the elastic case.

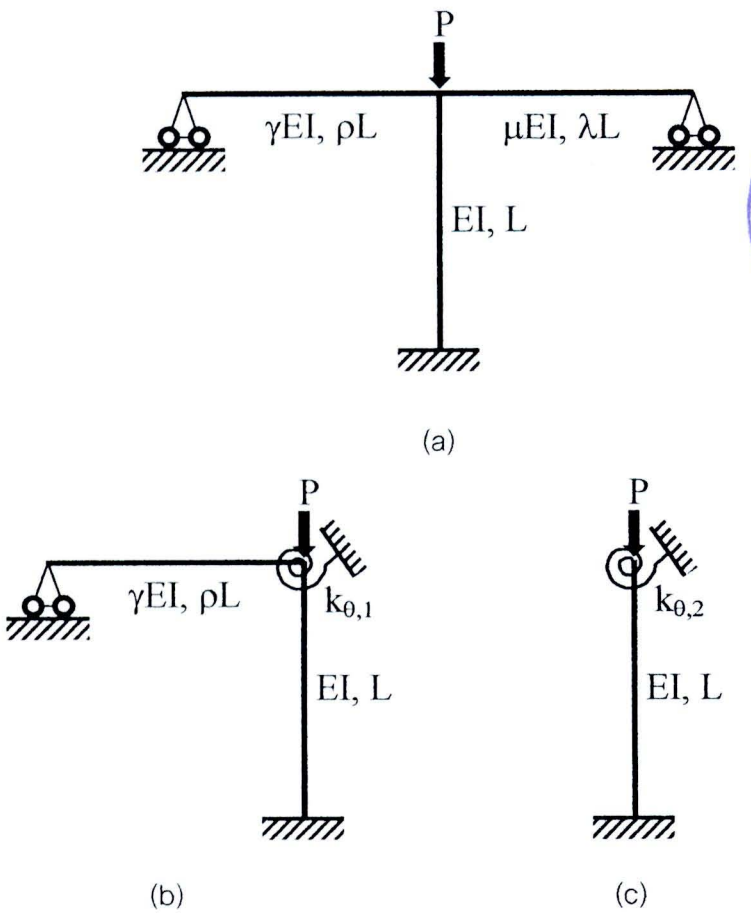

Figure 4.2 (a) Schematic of rigid frame subjected to vertical load P at top of column, (b) equivalent model obtained by replacing right beam by elastic rotational spring at top of column, and (c) equivalent model obtained by replacing left and right beams by elastic rotational spring at top of column

Table 4.7 Normalized computed elastic buckling loads of rigid frame using three different models compared with normalized exact solution

					Model (a)	Model (b)	Model (c)
γ	ρ	μ	λ	$\hat{P}_{exact}$	$\hat{P}_{current}$, (N, $\sum\tilde{n}$)	$\hat{P}_{current}$, (N, $\sum\tilde{n}$)	$\hat{P}_{current}$, (N, $\sum\tilde{n}$)
1	1	1	1	0.747665	0.747665 (3,12)	0.747665 (3,12)	0.747665 (3,12)
3	1	1	1	0.854549	0.854549 (3,12)	0.854549 (3,10)	0.854549 (3,10)
1	3	1	1	0.669441	0.669441 (3,12)	0.669441 (3,13)	0.669441 (3,12)
1	1	3	1	0.854549	0.854549 (3,12)	0.854549 (3,10)	0.854549 (3,10)
1	1	1	3	0.669441	0.669441 (3,12)	0.669441 (3,13)	0.669441 (3,12)
1	1	1	0.1	0.942198	0.942198 (4,12)	0.942198 (4,12)	0.942198 (4,12)
1	0.1	1	0.1	0.967510	0.967510 (4,11)	0.967510 (4,11)	0.967510 (4,11)

Table 4.8 Normalized computed inelastic buckling loads of rigid frame using three different models compared with normalized exact solution for n = 4 and B = 0.75

					Model (a)	Model (b)	Model (c)
γ	ρ	μ	λ	$\hat{P}_{exact}$	$\hat{P}_{current}$, (N, $\sum\tilde{n}$)	$\hat{P}_{current}$, (N, $\sum\tilde{n}$)	$\hat{P}_{current}$, (N, $\sum\tilde{n}$)
1	1	1	1	0.043988	0.043988 (7, 21)	0.043988 (7, 21)	0.043988 (7, 21)
3	1	1	1	0.044070	0.044070 (6,19)	0.044070 (6,19)	0.044070 (6,19)
1	3	1	1	0.043906	0.043906 (7, 21)	0.043906 (7, 21)	0.043906 (7, 21)
1	1	3	1	0.044070	0.044070 (6,19)	0.044070 (6,19)	0.044070 (6,19)
1	1	1	3	0.043906	0.043906 (7, 21)	0.043906 (7, 21)	0.043906 (7, 21)
1	1	1	0.1	0.044122	0.044122 (5,14)	0.044122 (5,14)	0.044122 (5,14)
1	0.1	1	0.1	0.044136	0.044136 (5,14)	0.044136 (5,14)	0.044136 (5,14)

4.3 Simply-support column braced by translational spring at its mid-span

Next, consider a simply-supported column of length 2L and flexural rigidity EI and being braced against the lateral movement at its mid-span by an elastic translational spring stiffness k as shown in Figure 4.3(a). This problem was solved analytically and reported by Timoshenko and Gere (1961). It was demonstrated that the buckling switches from a single curvature mode to a double curvature mode (similar to

Table 4.9 Normalized computed inelastic buckling loads of rigid frame using three different models compared with normalized exact solution for n = 8 and B = 0.875

					Model (a)	Model (b)	Model (c)
γ	ρ	μ	λ	$\hat{P}_{exact}$	$\hat{P}_{current}$, (N, $\sum\tilde{n}$)	$\hat{P}_{current}$, (N, $\sum\tilde{n}$)	$\hat{P}_{current}$, (N, $\sum\tilde{n}$)
1	1	1	1	0.026220	0.026220 (6, 20)	0.026220 (6, 20)	0.026220 (6, 20)
3	1	1	1	0.026234	0.026234 (6,18)	0.026234 (6,18)	0.026234 (6,18)
1	3	1	1	0.026205	0.026205 (7, 21)	0.026205 (7, 21)	0.026205 (7, 21)
1	1	3	1	0.026234	0.026234 (6,18)	0.026234 (6,18)	0.026234 (6,18)
1	1	1	3	0.026205	0.026205 (7, 21)	0.026205 (7, 21)	0.026205 (7, 21)
1	1	1	0.1	0.026243	0.026243 (5,14)	0.026243 (5,14)	0.026243 (5,14)
1	0.1	1	0.1	0.026246	0.026246 (5,14)	0.026246 (5,14)	0.026246 (5,14)

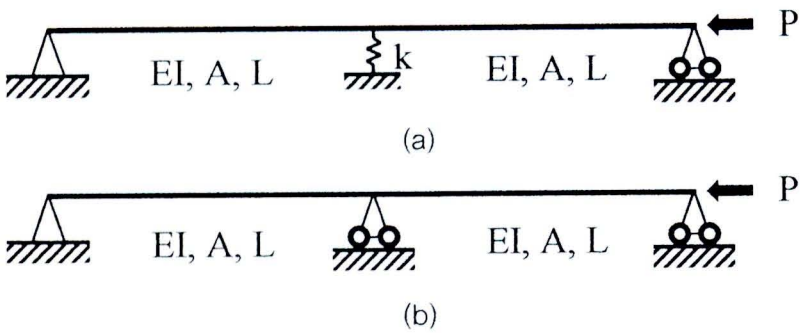

Figure 4.3 (a) Simply-supported column braced against lateral movement at its mid-span by translational spring and (b) two-span column with equal length

the buckling mode of a column shown in Figure 4.3(b)) when the spring stiffness k reaches the value $16\pi^2EI/(2L)^3$. In the analysis, the column is discretized into 2 equal elements and numerical results are shown in Table 4.10 for various values of normalized spring stiffness $\bar{k} = k/(\pi^2EI/(2L)^3)$ and in Figure 4.4 for the entire range of $\bar{k}$. As anticipated, converged buckling loads obtained from the current technique for various values of k are identical to the exact solution and the number of adaptive steps required is relatively low. In addition, the technique requires no additional treatment in order to accurately capture the mode switching. It should be pointed out, however, that when the

spring stiffness k close to the critical value (i.e. $16\pi^2EI/(2L)^3$), it is required the larger number of the iterations to compute the minimum eigenvalue.

Table 4.10 Normalized elastic buckling load of simply-supported column braced at its mid-span by translational spring with stiffness k. The number of adaptive steps (N) and the total number of iterations for eigenvalue computation ($\sum \tilde{n}$) are also reported

$\bar{k}$	N	$\sum \tilde{n}$	$\frac{P_{current}}{\pi^2EI/(2L)^2}$	$\frac{P_{exact}}{\pi^2EI/(2L)^2}$
0	3	12	1.000000	1.000000
4	4	15	1.798972	1.798972
8	4	24	2.570652	2.570652
12	4	37	3.307505	3.307505
16	4	55	4.000000	4.000000
20	5	183	4.000000	4.000000
40	5	27	4.000000	4.000000
100	5	21	4.000000	4.000000
∞	5	17	4.000000	4.000000

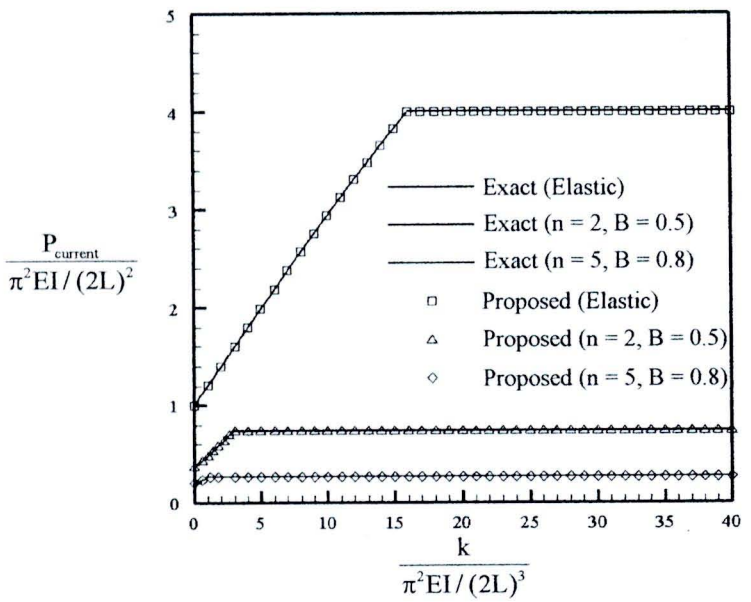

Figure 4.4 Normalized buckling load for simply-supported column braced at its mid-span by translational spring versus the normalized spring stiffness

Next, the inelastic buckling of the same structure is investigated. In the analysis, the reference stress σ_0 = 2812278.5 kg/m^2, the reference strain ε_0 = 0.00110938, I = 0.00013333 m^4, A = 0.04 m^2 and L = 1 m are employed. Numerical and exact solutions are presented in Table 4.11 for various values of $\bar{k}$ and in Figure 4.4 for the entire range of $\bar{k}$. In addition, the buckling shapes of the column for both elastic and inelastic cases are also reported in Figure 4.5 for certain values of $\bar{k}$, n and B. It is evident that for a small value of $\bar{k}$ (buckling in a single curvature mode), the buckling shapes for elastic and inelastic cases exhibit slight difference in the middle region of the column whereas, for a large value of $\bar{k}$ (buckling in a double curvature mode), the buckling shapes for all cases are identical.

Table 4.11 Normalized inelastic buckling load of simply-supported column braced at its mid-span by translational spring with stiffness k. The number of adaptive steps (N) and the total number of iterations for eigenvalue computation ($\sum \tilde{n}$) are also reported

$\bar{k}$	n = 2, B = 0.5				n = 5, B = 0.8			
	N	$\sum \tilde{n}$	$\frac{P_{current}}{\pi^2 EI/(2L)^2}$	$\frac{P_{Exact}}{\pi^2 EI/(2L)^2}$	N	$\sum \tilde{n}$	$\frac{P_{current}}{\pi^2 EI/(2L)^2}$	$\frac{P_{Exact}}{\pi^2 EI/(2L)^2}$
0	4	14	0.367266	0.367266	4	15	0.201358	0.201358
1	12	40	0.480689	0.480689	26	99	0.261131	0.261131
1.5	14	47	0.544713	0.544713	9	113	0.265694	0.265694
2	15	54	0.611299	0.611299	7	89	0.265694	0.265694
2.5	16	62	0.678074	0.678074	7	67	0.265694	0.265694
3	16	72	0.734532	0.734532	7	61	0.265694	0.265694
5	7	85	0.734532	0.734532	7	58	0.265694	0.265694
10	6	57	0.734532	0.734532	6	55	0.265694	0.265694
∞	6	20	0.734532	0.734532	6	26	0.265694	0.265694

4.4 Column resting on elastic foundation

Consider, next, the flexural buckling of a single column resting on an elastic two-parameter foundation as shown in Figure 4.6. This fourth example is chosen

to further verify the developed technique for the case that both the shear deformation and an elastic foundation are included in the mathematical model. For this particular problem, the exact buckling load is available for a column with the pinned-pinned end condition whereas the benchmark numerical solutions were presented by Seemapholkul (2000) for a column with both pinned-fixed and fixed-fixed end conditions.

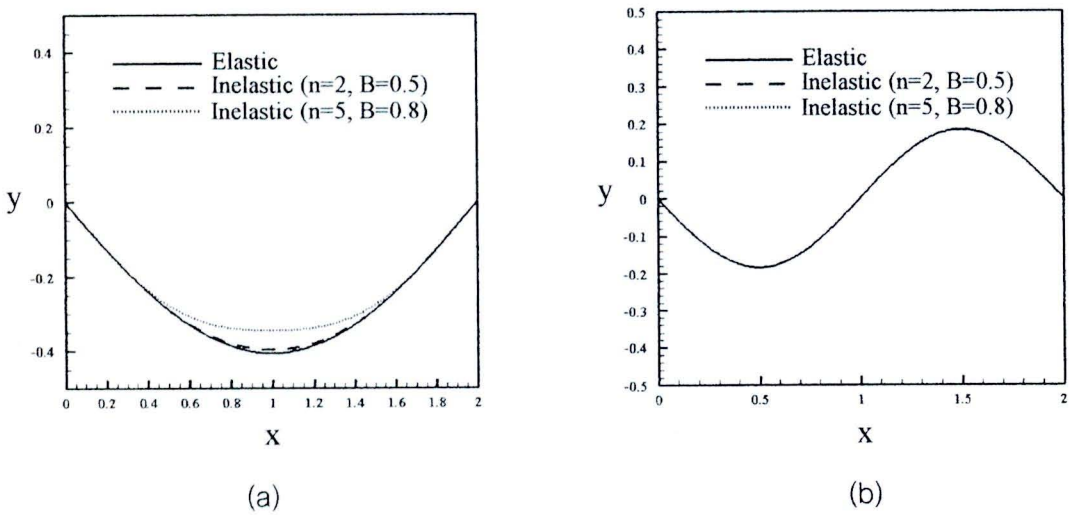

Figure 4.5 Buckling shape of simply-supported column braced at its mid-span by translational spring versus the normalized spring stiffness: (a) $\bar{k} = 1$ and (b) $\bar{k} = 20$

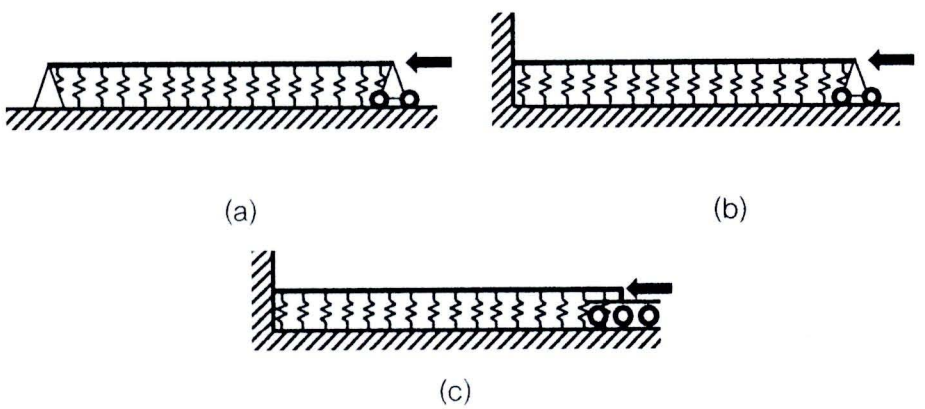

Figure 4.6 Schematic of column resting on an elastic two-parameter foundation with (a) pinned-pinned end condition, (b) pinned-fixed end condition, and (c) fixed-fixed end condition

In the modeling, only one element is used in the discretization for the pinned-pinned and fixed-pinned columns whereas 2 elements are utilized for the fixed-fixed column. In numerical experiments, essential parameters are chosen to be identical to those used by Seemapholkul (2000), for instance, E = 29,000 ksi, L/R = 100 in, I = 719 in^4, A = 32.9 in^2 and G = 11,600 ksi. Numerical results for the buckling load obtained for the three end conditions are reported in Table 4.12. It is evident that the converged buckling load for the pinned-pinned column predicted by the current technique is identical to the exact solution whereas those for the fixed-pinned and fixed-fixed columns show very good agreement with the benchmark numerical solutions. Again, only few adaptive steps are required to obtain such highly accurate numerical solutions.

Table 4.12 Computed buckling load of column resting on elastic foundation with three end conditions compared with exact solution (P_{exact}) and benchmark numerical solution (P_{ref}) presented by Seemapholkul (2000). The number of adaptive steps is also indicated in the parenthesis

λ	K_1 (ksi)	K_2 (kips)	Pinned-pinned column		Fixed-pinned column		Fixed-fixed column	
			$P_{current}$ (ksi), (N)	P_{exact} (ksi)	$P_{current}$ (ksi), (N)	P_{ref} (ksi)	$P_{current}$ (ksi) , (N)	P_{ref} (ksi)
0	0	0	941.66 (4)	941.66	1,926 (5)	-	3,767 (4)	-
0	3	1000	16,856 (6)	16,856	17,797 (5)	17,800	20,443 (5)	20,448
2/3	0	0	938.19 (4)	938.19	1,911 (4)	-	3,712 (5)	-
2/3	0	0	20,504 (6)	20,504	20,801 (6)	-	22,810 (6)	-
2/3	3	1000	16,583 (5)	16,583	17,432 (5)	17,359	19,745 (5)	19,710
2/3	5	100	20,604 (6)	20,604	20,901 (6)	-	22,910 (6)	-

4.5 One story portal frame

Consider next a one-story portal frame with geometry, cross-sectional properties, loading conditions shown in Figure 4.7. The Young modulus and shear modulus of both beams and frames are given by E and G with Poisson ratio = 0.25. The

In the modeling, only one element is used in the discretization for the pinned-pinned and fixed-pinned columns whereas 2 elements are utilized for the fixed-fixed column. In numerical experiments, essential parameters are chosen to be identical to those used by Seemapholkul (2000), for instance, E = 29,000 ksi, L/R = 100 in, I = 719 in^4, A = 32.9 in^2 and G = 11,600 ksi. Numerical results for the buckling load obtained for the three end conditions are reported in Table 4.12. It is evident that the converged buckling load for the pinned-pinned column predicted by the current technique is identical to the exact solution whereas those for the fixed-pinned and fixed-fixed columns show very good agreement with the benchmark numerical solutions. Again, only few adaptive steps are required to obtain such highly accurate numerical solutions.

Table 4.12 Computed buckling load of column resting on elastic foundation with three end conditions compared with exact solution (P_{exact}) and benchmark numerical solution (P_{ref}) presented by Seemapholkul (2000). The number of adaptive steps is also indicated in the parenthesis

λ	K_1 (ksi)	K_2 (kips)	Pinned-pinned column		Fixed-pinned column		Fixed-fixed column	
			$P_{current}$ (ksi), (N)	P_{exact} (ksi)	$P_{current}$ (ksi), (N)	P_{ref} (ksi)	$P_{current}$ (ksi) , (N)	P_{ref} (ksi)
0	0	0	941.66 (4)	941.66	1,926 (5)	-	3,767 (4)	-
0	3	1000	16,856 (6)	16,856	17,797 (5)	17,800	20,443 (5)	20,448
2/3	0	0	938.19 (4)	938.19	1,911 (4)	-	3,712 (5)	-
2/3	0	0	20,504 (6)	20,504	20,801 (6)	-	22,810 (6)	-
2/3	3	1000	16,583 (5)	16,583	17,432 (5)	17,359	19,745 (5)	19,710
2/3	5	100	20,604 (6)	20,604	20,901 (6)	-	22,910 (6)	-

4.5 One story portal frame

Consider next a one-story portal frame with geometry, cross-sectional properties, loading conditions shown in Figure 4.7. The Young modulus and shear modulus of both beams and frames are given by E and G with Poisson ratio = 0.25. The

Table 4.13 Normalized elastic buckling load ($P_{current}$) of one-story portal frame shown in Figure 4.4. Results are compared with exact solutions (P_{exact}) and benchmark solution (P_{FEM}) from FEM

α	β	ρ	γ	μ	No shear deformation		With column shear deformation	
					$\frac{P_{current}}{\pi^2 EI/L^2}$, (N)	$\frac{P_{exact}}{\pi^2 EI/L^2}$	$\frac{P_{current}}{\pi^2 EI/L^2}$, (N)	$\frac{P_{FEM}}{\pi^2 EI/L^2}$
1	1	1	1	1	0.747665 (3)	0.747665	0.696285 (4)	0.696506
5	1	1	1	1	1.434923 (4)	1.434923	1.229010 (5)	1.229351
1	5	1	1	1	0.936730 (4)	0.936730	0.857457 (3)	0.858177
1	1	5	1	1	0.247925 (4)	0.247925	0.229675 (4)	0.229879
1	1	1	5	1	0.443284 (3)	0.443284	0.424703 (4)	0.424821
1	1	1	1	5	0.747665 (3)	0.747665	0.716359 (3)	0.716851
5	1	0.1	1	1	2.553626 (4)	2.553626	2.115826 (6)	2.116454
1	1	0.1	1	5	1.348748 (4)	1.348748	1.283583 (4)	1.284468

Table 4.14 Normalized inelastic buckling load ($P_{current}$) of one-story portal frame shown in Figure 4.4. Results are compared with exact solutions (P_{exact})

α	β	ρ	γ	μ	No shear deformation			
					n =3, B = 2/3		n =4, B = ¾	
					$\frac{P_{current}}{\pi^2 EI/L^2}$, (N)	$\frac{P_{exact}}{\pi^2 EI/L^2}$	$\frac{P_{current}}{\pi^2 EI/L^2}$, (N)	$\frac{P_{FEM}}{\pi^2 EI/L^2}$
1	1	1	1	1	0.137838 (7)	0.137838	0.108516 (7)	0.108516
3	1	1	1	1	0.169497 (9)	0.169497	0.127253 (9)	0.127253
1	3	1	1	1	0.139310 (6)	0.139310	0.109194 (6)	0.109194
1	1	3	1	1	0.073092 (18)	0.073092	0.051308 (27)	0.051308
1	1	1	3	1	0.133370 (10)	0.133370	0.106430 (10)	0.106430
1	1	1	1	3	0.137838 (7)	0.137838	0.108516 (7)	0.108516
3	1	0.3	1	1	0.219724 (19)	0.219724	0.154005 (23)	0.154033
1	1	0.3	1	3	0.219412 (16)	0.219412	0.153920 (22)	0.153948

Table 4.14 (Cond.) Normalized inelastic buckling load ($P_{current}$) of one-story portal frame shown in Figure 4.4. Results are compared with exact solutions (P_{exact})

α	β	ρ	γ	μ	No shear deformation	
					n =5, B = 4/5	
					$\frac{P_{current}}{\pi^2 EI / L^2}$, (N)	$\frac{P_{exact}}{\pi^2 EI / L^2}$
1	1	1	1	1	0.093911 (7)	0.093911
3	1	1	1	1	0.106851 (9)	0.106851
1	3	1	1	1	0.094315 (6)	0.094315
1	1	3	1	1	0.041403 (35)	0.041415
1	1	1	3	1	0.092661 (9)	0.092661
1	1	1	1	3	0.093911 (7)	0.093911
3	1	0.3	1	1	0.124251 (13)	0.124294
1	1	0.3	1	3	0.124210 (32)	0.124261

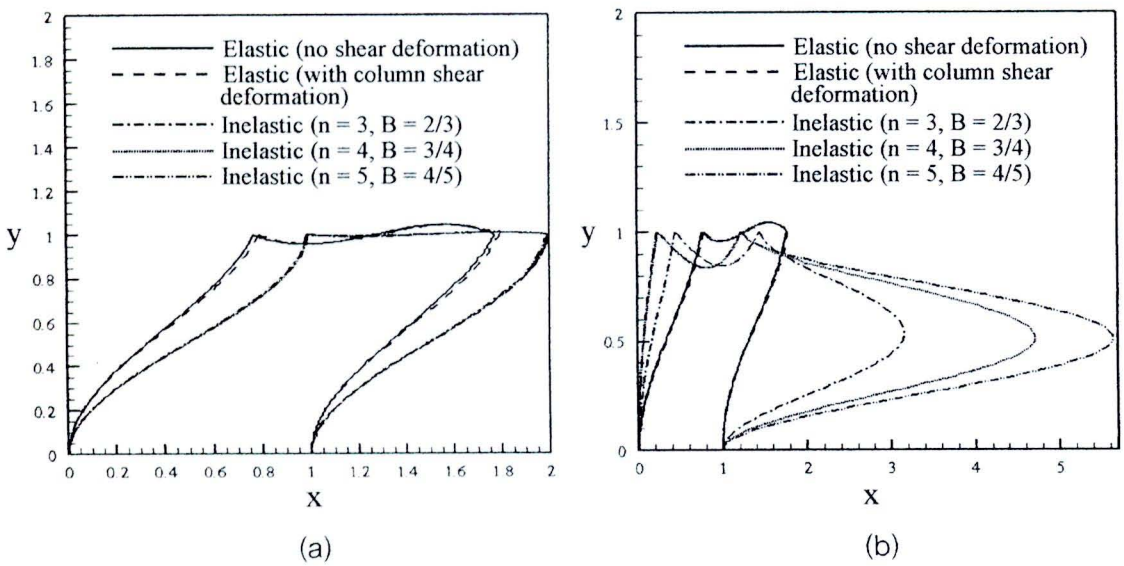

Figure 4.8 Buckling shapes of one story portal frame: (a) {α, β, ρ, γ, μ} = {1, 1, 1, 1, 1} and (b) {α, β, ρ, γ, μ} = {1, 1, 5, 1, 1} for elastic buckling and {α, β, ρ, γ, μ} = {1, 1, 3, 1, 1} for inelastic buckling

span length of each bay and the height of each levels are given by {2L, L, 2L} and {L, L, L, L, L}, respectively. The moment of inertia and the cross-sectional area of columns in

the first to fifth levels are given by {3I, 2I, 2I, I, I} and {3A, 2A, 2A, A, A}, respectively, whereas the moment of inertia and the cross-sectional area of all beams are given by I and A, respectively. The Young modulus and shear modulus of both beams and columns are given by E and G and the Poisson ratio is taken to be 0.25. In the analysis, the frame is discretized in to 35 members (20 elements for columns and 15 elements for beams) and I = 0.000675 m^4, λ = 0.8331, A = 0.09 m^2 and L = 1 m are employed. The normalized elastic buckling load of the frame, denoted by $\hat{P}_{current}=P_{current}/(\pi^2 EI/L^2)$, with and without shear deformation for various values of normalized spring stiffness, denoted by $\bar{k}=k/(\pi^2 EI/(2L)^3)$, are reported and compared with benchmark solutions obtained from a reliable FEM package in Figure 4.10. The buckling shapes of this frame are also reported in Figure 4.11 for certain values of $\bar{k}$. It is apparent that when the spring stiffness k reaches a certain finite value, the buckling load is identical to that of the same frame being fully fixed against the side-sway (i.e. k = ∞). Again, the switch of buckling modes can be accurately captured by the current technique. Note in addition that the shear deformation significantly lowers the flexural buckling load of this particular frame but insignificantly influences the buckling shape.

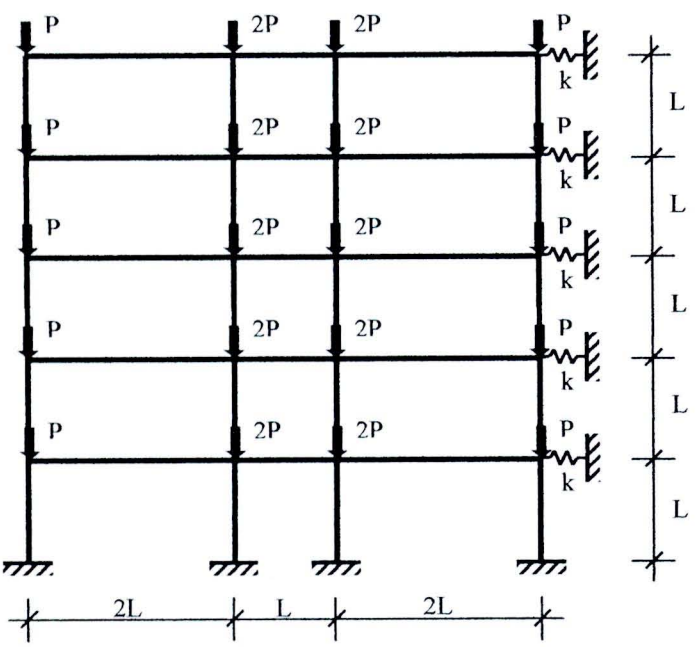

Figure 4.9 Schematic of axially-loaded, multi-story frame with side-sway restraints

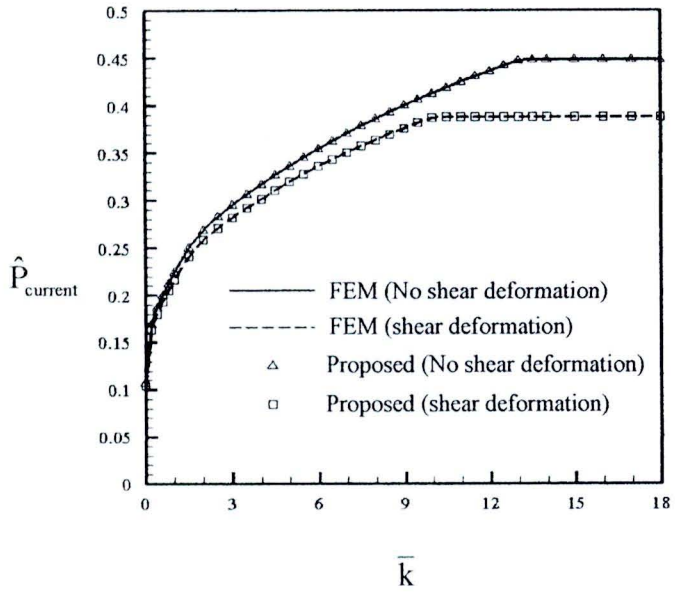

Figure 4.10 Normalized elastic buckling load of axially loaded, multi-story frame with side-sway restraints versus normalized spring stiffness

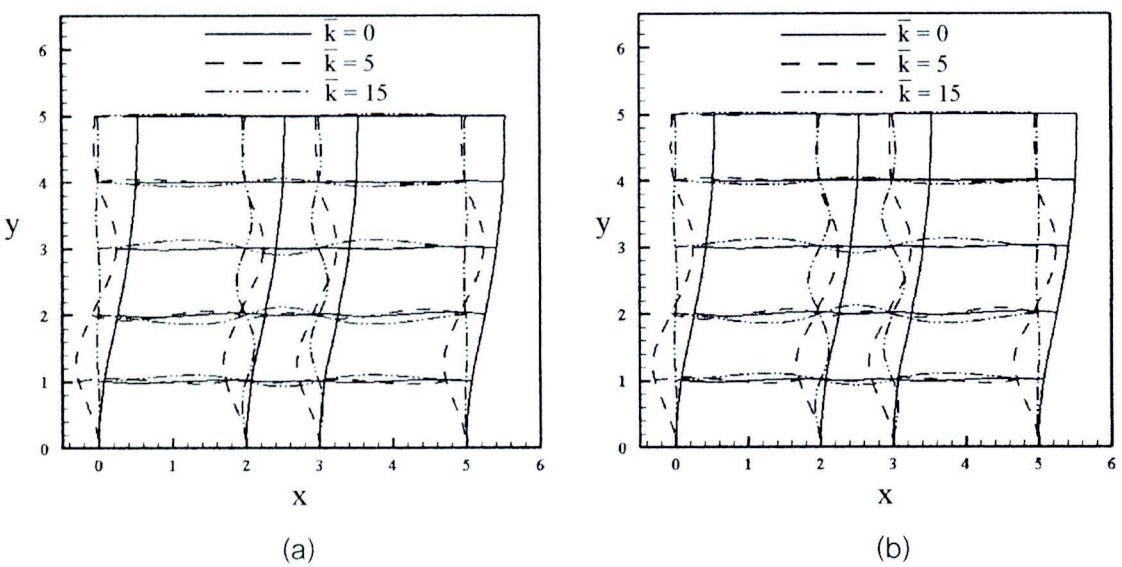

Figure 4.11 The buckling shapes of multi-storey frame with side-sway restraint: (a) without shear deformation and (b) with shear deformation